Rigorous and efficient optical VCSEL model based on vectorial eigenmode expansion and perfectly matched layers

Peter Bienstman, *Student Member, IEEE*, Roel Baets, *Senior Member, IEEE*

Abstract— **We present a novel optical VCSEL model based on vectorial eigenmode expansion combined with perfectly matched layer (PML) boundary conditions. It is fully rigorous and computationally efficient, as the PML boundaries eliminate parasitic reflections and allow the metal discretization wall to be placed much closer to the device under study. The model is illustrated with a number of simulation results on proton-implanted, airpost, oxide-confined and tapered oxide VCSELs. The trade-off between tight transverse optical confinement and scattering loss is clearly illustrated, as is the influence of the gain profile.**

Keywords— **Distributed Bragg reflector lasers, laser modes, semiconductor device modeling, semiconductor lasers, surface-emitting lasers**

I. Introduction

In recent years, the characteristics of vertical-cavity surface-emitting lasers (VCSELs) have improved enormously, especially after the introduction of oxidized apertures to realize electrical and optical confinement. Today's VCSELs show low threshold current densities [1] and high output powers. Moreover, their circular beam profiles and the possibility to integrate then into 2D arrays [2] make them suitable candidates for short-range optical communication and optical interconnect.

In order to design next generation VCSELs with even better performance, it is imperative to be able to model the optical, electrical and thermal effects that come into play in these devices. Specifically the modeling of the optical field is quite challenging, since the Helmholtz equation is not separable in this case. Moreover, these structures can have large index contrasts, especially so for oxide-confined and airpost VCSELs. Over the years, a number of approaches have been proposed to model VCSELs, either scalar or vectorial, or approximate or rigorous (see [3] and references therein).

Although scalar and approximate models can yield accurate approximations, rigorous vectorial models become preferable for small devices with large index contrasts, or when studying the polarization properties of VCSELs. Currently, most vectorial optical VCSEL models are based on some form of spatial discretization, e.g. finite differences or finite elements ([4], [5]). However, in order to give sufficiently accurate results, the discretization grid has to be very fine, which can lead to a very significant computational effort.

The authors are with the Department of Information Technology (INTEC), Ghent University / IMEC, Sint-Pietersnieuwstraat 41, B-9000 Gent, Belgium, tel +32 9 264 33 16, fax +32 9 264 35 93, E-mail: Peter.Bienstman@rug.ac.be

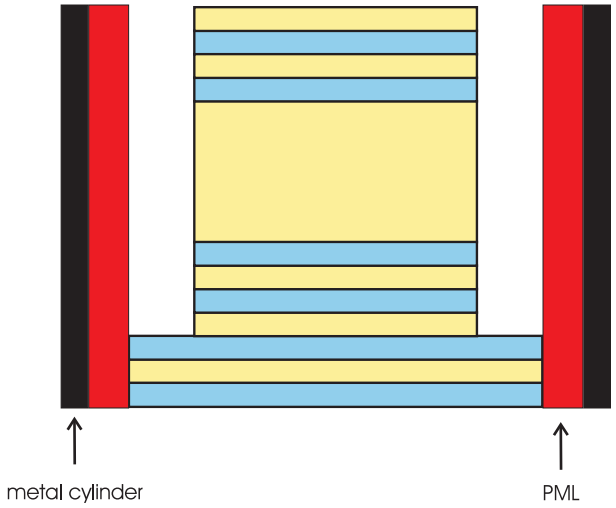

Fig. 1. VCSEL enclosed by a metal cylinder clad with PML

The eigenmode expansion method we introduced in [6] is numerically much more efficient, as it does not rely on spatial discretization, but rather expands the VCSEL field in each longitudinally invariant layer in terms of the eigenmodes of that particular layer. However, in order to get a discrete set of radiation modes, the VCSEL has be enclosed by a metal cylinder with perfectly conducting walls. This means that diffraction or scattering inside the VCSEL will give rise to radiation that will be totally reflected at the metal cylinder. These parasitic reflections will come back to the structure under study and can seriously disturb the simulation results [7]. In theory, we can reduce the influence of these parasitic reflections by choosing the radius of the discretization cylinder very large. However, this leads to an increased computational effort, because the larger computational volume means we have to include more modes to achieve convergence.

In this paper, we discuss an improved VCSEL model, where we alleviate this problem by coating the inside of the metal wall with a perfectly matched layer (PML) [8] (fig. 1). In this way parasitic reflections are significantly reduced, leading to an improved accuracy and shorter run times, as we can now place the metal wall much closer to the VCSEL under study.

The remainder of this paper is structured as follows. In section II, we outline the principles underlying the optical model. Section III discusses the simulation results obtained by this model for a large variety of devices, ranging from

proton-implanted VCSELs over airpost devices, to oxide-confined and tapered oxide VCSELs.

II. Description of the model

The model proceeds along a number of steps. First of all, the structure inside the PML-clad metal cylinder is divided into a number of layers where the index profile does not change in the propagation direction. In each of these layers, we expand the field in the eigenmodes of that particular layer. As we already explained in [8], PML is incorporated by allowing the cladding of the waveguide to assume a complex thickness. The imaginary part of this complex thickness provides for reflectionless absorption of the incident field, regardless of wavelength, incidence angle or polarization, which is a significant advantage compared to other boundary conditions [9]. We opt for the complex coordinate formulation of PML [10], rather than for the anisotropic material formalism [11], as the former allows us to easily extend all our existing analytic formulas from the non-PML case, simply by letting all the cladding thickness assume complex values. The eigenmodes in the presence of PML are then found by solving a dispersion relation in the complex plane. Contrary to our previous model [6], we solve for these eigenmodes directly, rather than indirectly expanding these eigenmodes in turn on the eigenmodes of a uniform cross-section. By working directly with the dispersion relation for non-uniform cross-sections, we improve the accuracy and speed of the procedure.

With the knowledge of the propagation constants and field profiles of the eigenmodes in each layer, we can proceed to calculate the scattering matrix (i.e. reflection and transmission matrices) of the interfaces between two layers using the well-known mode-matching technique. Subsequently, we can calculate the scattering matrix for an entire stack of layers using the S-scheme formalism. All of this was presented in more detail in [7].

With this information we can finally start locating VCSEL modes, which are of course resonant optical field distributions that can propagate indefinitely back and forth inside the cavity without the need for any external sources. To formulate this mathematically, we start by dividing the cavity at an arbitrary location in a top and a bottom part (fig. 2). Using the techniques discussed above, we calculate the reflection matrix $\mathbf{R_{top}}$ of the top part as seen from the bottom, and similarly the reflection matrix $\mathbf{R_{bot}}$ of the bottom part as seen from the top. Describing the laser mode by its (so far unknown) eigenmode expansion coefficients collected in the vector $\mathbf{A_{lasing}}$, we can express the condition of unity round trip gain as

$$\mathbf{R_{top}} \cdot \mathbf{R_{bot}} \cdot \mathbf{A_{lasing}} = \mathbf{A_{lasing}} \tag{1}$$

Put differently, if the cavity matrix $\mathbf{Q} = \mathbf{R_{top}} \cdot \mathbf{R_{bot}}$ has an eigenvector with an eigenvalue ν of 1, this eigenvector describes a lasing mode.

For an arbitrary structure, $\mathbf{Q}$ will not have such an eigenvector. We will need to vary the wavelength λ to get phase resonance, which is when the eigenvalue ν lies on the positive real axis. In the absence of any gain in the active region, ν will be smaller than unity, because of the losses inside the cavity. This means that we will also have to tune the material gain g_{mat} in the active region, in order to achieve amplitude resonance, where the gain exactly compensates the losses. We do this by simply changing the imaginary part of the refractive index of the gain area, which is by definition related to g_{mat} by

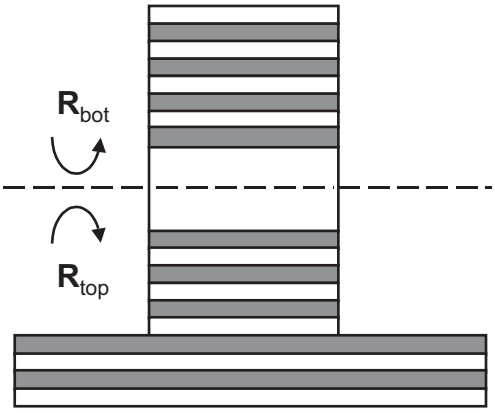

Fig. 2. Generic laser cavity consisting of a top and a bottom part.

$$g_{mat} = 2\frac{2\pi}{\lambda}\Im\left(n_{active}\right) \tag{2}$$

In summary, locating a laser mode consists of doing a search in the two-dimensional (λ, g_{mat}) space to find a point where $\mathbf{Q}$ has an eigenvector with an eigenvalue of 1. This gives the laser mode's resonance wavelength, threshold material gain and field profile. Also note that the exact location of the gain region(s) with respect to the cavity cut is completely arbitrary.

Finally, we want to point out that in practice, we do not really need to perform a search in a 2D space to achieve resonance. It turns out that in the vast majority of cases, we can suffice by doing a sequence of 1D searches. Keeping the gain fixed at zero, we first vary the wavelength until we arrive at phase resonance. Subsequently, we keep the wavelength fixed and increase the material gain until we locate the laser mode. If we need higher precision, we can continue to vary wavelength and gain around this point, but usually, we can get a precision on the order of 10^{-4} with one wavelength and one gain sweep.

Using 100 modes, the entire process of finding the wavelength and gain of a laser mode typically takes only about five minutes on a Sun UltraSparc II 250 MHz. This VCSEL model is incorporated in our optical modeling framework CAMFR [7], which can o.a. also be used to model photonic crystal devices.

III. Transverse confinement in VCSELs

Different types of VCSELs are mainly distinguished by the way in which they realize transverse optical confinement. Over the past few years, several approaches to achieve transverse confinement have been tried out experimentally, some of which now well-established, others more speculative and research-oriented. We will now com-

	d (nm)	Material	Refr. index
air		air	1.00
25 pair DBR	69.49	GaAs	3.53
	79.63	AlGaAs	3.08
	136.49	GaAs	3.53
lambda cavity	5.0	QW	3.53+...j
	136.49	GaAs	3.53
29.5 pair DBR	79.63	AlGaAs	3.08
	69.49	GaAs	3.53
substrate		GaAs	3.53

TABLE I
LAYER STRUCTURE OF THE COST VCSEL.

pare many of these approaches numerically, which will show among others that designing transverse confinement in VCSELs is not a trivial matter, because it involves some trade-offs and because its design cannot be separated from that of the rest of the cavity.

A. Proton-implanted VCSELs

Proton implantation achieves confinement by selectively bombarding areas of the substrate with protons. This destroys the lattice structure of the semiconductor, turning the exposed regions into an isolator. By leaving circular apertures free from implantation, conducting regions surrounded by isolators can be created, which funnel the injected current into a small area in the active region [12].

Proton implantation does not change the optical properties of the exposed regions appreciably, so the only refractive index change in the VCSEL is the localized gain in the active region below the aperture due to current injection. Since this is a very small confining effect, thresholds in these devices tend to be relatively high.

To illustrate this, we calculated the threshold material gain as a function of aperture size for the VCSEL layer structure from table I. It is an AlGaAs VCSEL designed for emission around 980 nm. The cavity is one optical wavelength long, has 29.5 bottom DBR pairs and 25 top DBR pairs. It has a single 5 nm thick quantum well (QW) as an active region. The gain profile is taken to be piecewise constant. Inside the aperture, there is a constant gain, with a level to be determined by the laser mode locating algorithm. Outside the aperture, there is a small constant loss, indicated by an imaginary refractive index of -0.01. This structure is not chosen to mimic a realistic VCSEL design in all of its details, but rather as an illustration of the fundamental optical processes at work in VCSELs. As it was used in the COST268 modeling comparison [3], we will refer to this layer structure as the COST layer structure. All simulations in this paper were performed retaining 100 modes in the eigenmode expansion and placing the VCSEL in a metal cylinder with radius 12-0.05j μm, which proved to be more than enough in order to achieve convergence.

We can see from the results in fig. 3 that the threshold material gain quickly increases for decreasing aperture sizes. The results are plotted for the fundamental mode,

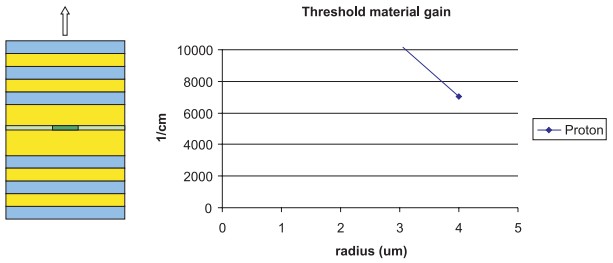

Fig. 3. Threshold material gain for the proton-implanted VCSEL.

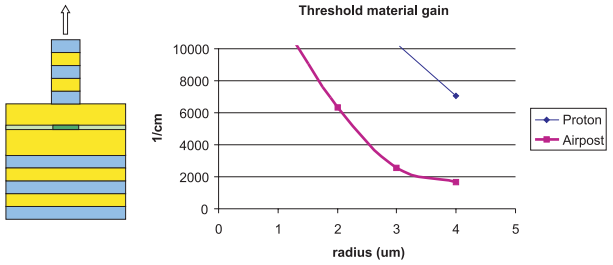

Fig. 4. Threshold material gain for the airpost VCSEL.

i.e. the HE_{11} mode (the lowest order mode with Bessel order 1). The trends from this figure can easily be explained as follows. As the device size decreases, diffraction effects will become more prominent and will cause the laser beam to spread out. After reflecting at the DBRs, the mode will have a size much larger than the pumped gain region, and this poor overlap of the optical mode with the gain profile will lead to a very inefficient amplification process of the laser beam.

Because the gain-guiding offers only a very weak confinement, these *diffraction losses* will quickly lead to very high thresholds for small devices. From fig. 3 and also from experimental evidence, we can therefore conclude that proton-implanted VCSELs with small diameters are not really feasible.

B. Airpost VCSELs

A second approach to achieve confinement in VCSELs is etching away the semiconductor material around the cavity to leave an airpost standing [13]. As this airpost acts as a waveguide offering strong confinement to the optical field, we expect the diffraction losses to be lower. This is illustrated by the simulation results from fig. 4. The 'background' VCSEL structure is the same as from table I, to allow easy comparison between the different forms of optical confinement. The gain diameter is taken to be the same as the post diameter. Clearly, the airpost VCSEL has much lower thresholds, making lasing in devices with a radius down to 3 μm feasible.

C. Thick-oxide-confined VCSELs

The most popular way of achieving lateral confinement nowadays is the use of aluminum oxidation. This process was first described in [14] and consists of etching an airpost to expose a semiconductor layer with high Al content, like e.g. $Al_xGa_{1-x}As$ with the Al fraction x larger than

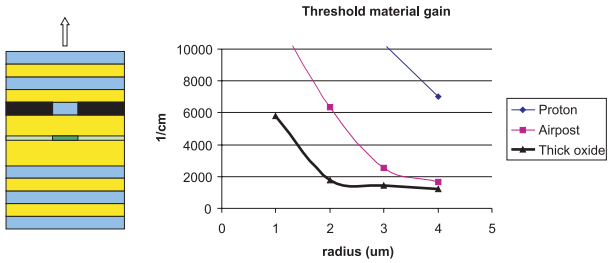

Fig. 5. Threshold material gain for the thick oxide aperture VCSEL.

90%. The sample is subsequently introduced in a furnace at a temperature of around 400 degrees, through which a steady flow of water vapor is maintained. This hydrogen-rich environment will laterally oxidize the exposed AlGaAs layer. This creates a current aperture, that can be used to restrict current injection to a small region in the active layer. Also, AlOx has a refractive index of around 1.55, which means that the oxide aperture will also act as a waveguide counteracting the diffraction losses.

Fig. 5 plots the threshold material gain of the reference VCSEL from table I, but this time with the bottom layer of the top DBR replaced by a partially oxidized $\lambda/4$ thick AlGaAs layer. The gain diameter is taken to be the same as the oxide diameter. We make abstraction of the airpost that was etched to expose this layer, because this post typically has a diameter much larger than that of the oxide aperture itself. It will therefore not affect the optical field appreciably.

From fig. 5 it is apparent that this oxide aperture performs even better than the airpost VCSEL. At first sight this might seem surprising, because the oxide clearly has a much smaller confining effect than the airpost: the confining effect is only present in a single layer and the refractive index contrast is lower.

This discrepancy can easily be explained by the increased scattering losses that occur in the airpost VCSEL as compared to the oxide VCSEL. To illustrate this, we plot the field profiles in an oxide-confined and an airpost VCSEL with a radius of 1 μm. These figures show the magnitude of the E_ϕ component of the optical field on a logarithmic scale. The left-hand edge of the figures is the symmetry axis $\rho = 0$, meaning that only the right half of the cavity is shown. Although the airpost achieves much better confinement in the top DBR, a lot of the light is lost at the corner interface between the unetched region, the etched airpost and the surrounding air layer. There, the light radiates out of the cavity in a wave traveling to the top right of the picture. For the oxide aperture, the weaker index contrast results in reduced scattering losses. At the same time however, the confinement is not as good, leading to higher diffraction losses. In this case, the balance between these two effects is such that the oxide-confined VCSEL has a lower threshold material gain than the airpost VCSEL.

In general, we can say that introducing any confining structure into a VCSEL will have two effects, one positive and one negative. On one hand, it will keep the optical field

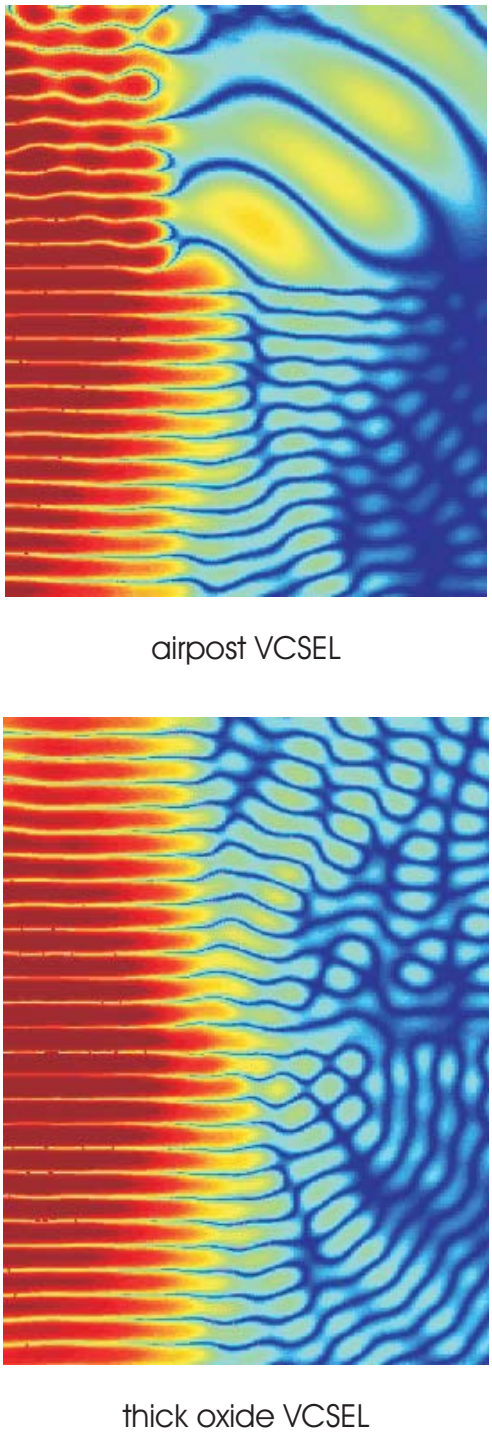

Fig. 6. Field profiles in an airpost VCSEL and a thick oxide VCSEL (the left edge of the figure is the rotational symmetry axis).

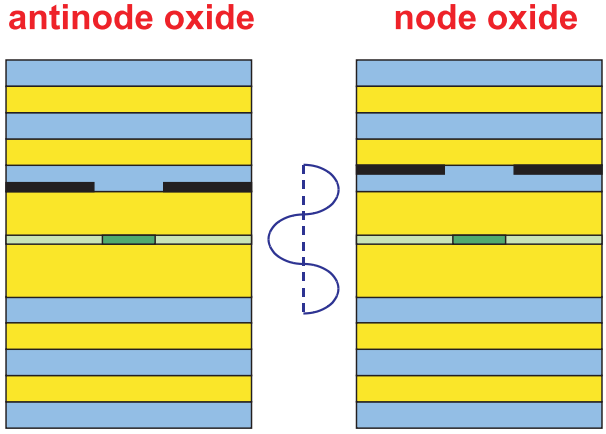

Fig. 7. VCSEL with a thin oxide aperture at an antinode or a node position.

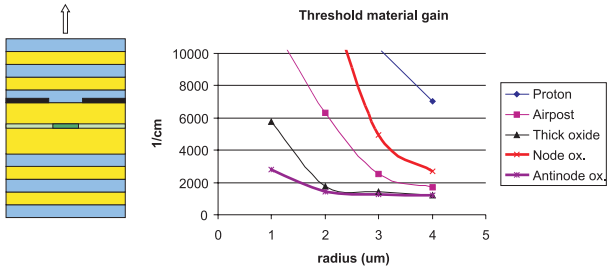

Fig. 8. Threshold material gain for the thin oxide VCSEL.

together when it is *inside* the confining structure, leading to reduced diffraction losses. On the other hand, coupling light into and out of this confining element disturbs the field and can lead to scattering losses at the *edges* of the structure. These effects tend to oppose each other in the sense that structures providing tight confinement also exhibit rather high scattering, so there is a fine balance to be struck.

D. Thin oxide-confined VCSELs

D.1 Aperture position dependent effects

This trade-off between diffraction and scattering losses leads to the reasoning behind the use of oxide apertures that are thinner than a quarter-wavelength layer. We can sacrifice some optical confinement by reducing the thickness of the oxide layer, which is compensated by a reduction in scattering loss since the thinner oxide will disturb the optical field less.

By reducing the thickness of the oxide layer, we also gain an additional degree of freedom, namely the position of the aperture with respect to the optical field. Fig. 7 illustrates how the aperture can be placed at either a maximum (antinode) or a minimum (node) of the optical field. In fig. 8, we show the threshold material gain for a node and an antinode aperture VCSEL with a thickness of $\lambda/20$, i.e one-fifth of the quarter-wavelength layer. Once again, the background VCSEL structure is the same. For the antinode oxide, the thresholds are the lowest of the devices we studied so far, clearly showing that the reduction in scattering losses outweighs the small loss of confinement. For the node oxide, the situation is very different. Because it is placed at a field minimum, it will hardly have any effect on the optical mode, meaning low scattering but also very poor optical confinement, leading to an optical field profile that is spread out considerably. The latter effect is much stronger in this case, so the thresholds of this device are quite high.

	d (nm)	Material	Refr. index
air		air	1.00
28 pair DBR	69.8	GaAs	3.51
	81.4	$Al_{.87}Ga_{.13}As$	3.01
	349.0	GaAs	3.51
node oxide	30.0	AlOx/AlAs	1.55/2.93
	30.0	$Al_{.27}Ga_{.73}As$	3.36
QW	8.0	InGaAs	3.51+...j
	30.0	$Al_{.27}Ga_{.73}As$	3.36
	120.0	$Al_{.50}Ga_{.50}As$	3.22
etch stop layer	558.4	GaAs	3.51
31.5 pair DBR	83.6	AlAs	2.93
	69.8	GaAs	3.51
substrate		GaAs	3.51

TABLE II
LAYER STRUCTURE OF THE NODE OXIDE USC VCSEL.

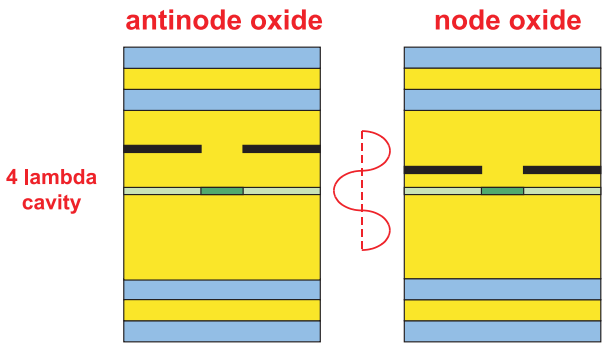

Fig. 9. USC VCSEL structure.

D.2 Influence of carrier diffusion

In the VCSEL structures we modeled so far, the antinode oxide always outperformed the node oxide in terms of threshold material gain. However, in some reports in literature, we can find devices where exactly the opposite behavior is seen experimentally. One example of this is a study performed at the University of Southern California at Los Angeles (USC) [15]. In this section, we will try to elucidate these apparent differences between theory and experiment.

The USC device has a very different structure than the COST VCSEL, so it is not advisable to extrapolate its behavior from that of the COST device, at least not intuitively without rigorous simulations. The USC layer structure is given in table II, and the main differences with the COST structure are illustrated in fig. 9.

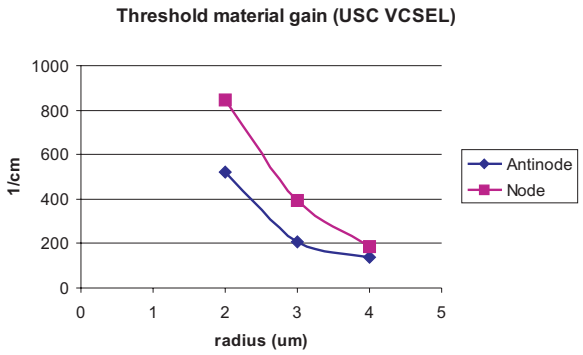

Fig. 10. Threshold material gain the the USC thin oxide VCSELs.

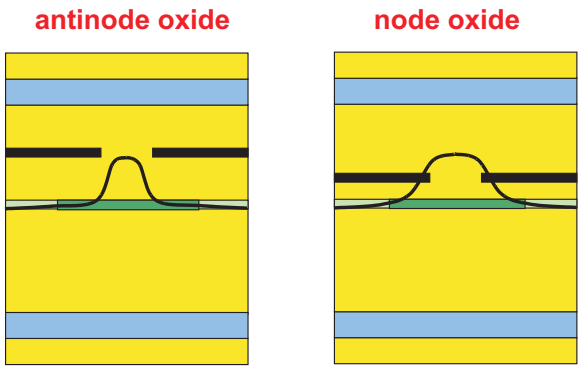

Fig. 11. Influence of lateral carrier diffusion on the overlap of the gain profile with the optical mode.

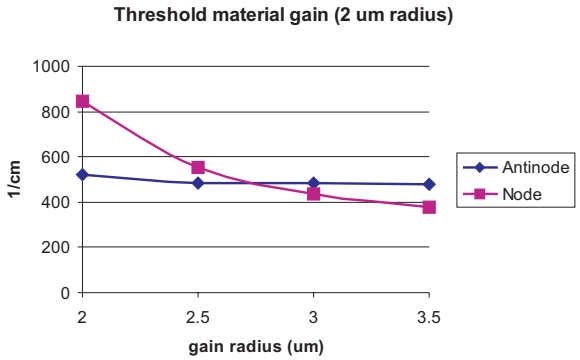

Fig. 12. Threshold material gain for the USC VCSELs with a 2 μm oxide aperture radius.

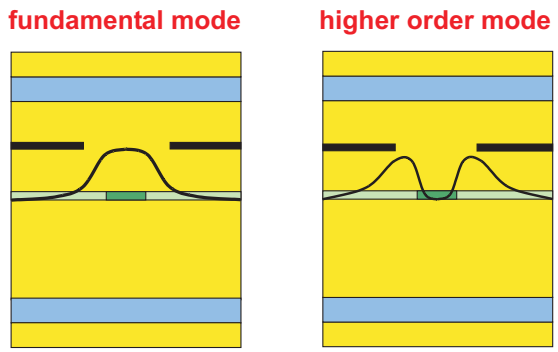

Fig. 13. VCSEL combining both a proton-implantation and an oxide aperture to increase the modal stability.

The device has a cavity length of 4λ, rather than the short 1λ devices we considered so far. Diffraction losses will therefore play a larger role in these longer cavities. Additionally, the USC node oxide is placed at the first field minimum, whereas the COST node aperture is placed at the second field minimum (fig. 7).

Fig. 10 shows the simulated thresholds for the USC devices. The relative threshold difference between the node and the antinode devices is smaller than in fig. 8, but still, the antinode device has a lower threshold, contrary to the experimental evidence. The difference in cavity design is therefore not sufficient to explain the observed experimental trends.

Clearly, another effect is important here, which is carrier diffusion as already suggested in [15]. Once carriers get injected through the oxide aperture inside the quantum wells, they tend to diffuse laterally. This means that the effective gain region will have a diameter larger than the oxide aperture diameter (fig. 11). We know that the lower optical confinement in the node oxide will cause the laser mode to spread. This larger modal cross-section is very well matched to the larger gain diameter caused by carrier diffusion (fig. 11). For the antinode oxide, the opposite is true. The mode profile is rather narrow, meaning that a significant fraction of the gain in the QW only sees the tail regions of the optical mode. Because of the low field intensity in these tails, pumping is very inefficient there and this fraction of the gain is effectively wasted.

We can quite easily simulate the effects of carrier diffusion by choosing the gain diameter larger than the oxide aperture diameter. The precise size of the gain region should follow from other non-optical models (carrier diffusion models), so we will just treat the gain diameter as a phenomenological parameter here and simulate the device for a number of values of the gain diameter. Fig. 12 shows the results of such simulations for devices with a 2 μm radius oxide aperture. We can clearly see that the node oxide starts to outperform the antinode oxide from a gain radius of 3 μm, i.e. a diffusion length of about 1 μm. These values are in the same range as those reported in [15], which indicates that lateral carrier diffusion is indeed the relevant effect explaining the experimental trends.

E. Proton-implanted oxide-confined VCSELs

The effects of the gain diameter size relative to the oxide diameter size are exploited to increase modal stability in VCSELs which combine both a proton-implant and an oxide aperture [16]. The diameter of the proton-implant aperture is chosen to be smaller than that of the oxide aperture, such that the effective gain diameter is also smaller than the oxide diameter (fig. 13). Such a device layout will significantly increase the threshold of the higher order modes (e.g. the TE_{01} mode, the lowest order mode with Bessel order 0 and TE polarization) with respect to the fundamental mode. This is immediately clear from fig. 13, because for the higher order mode, almost all the gain is concentrated in regions where the optical field is very low. This high modal stability can lead to high-power devices

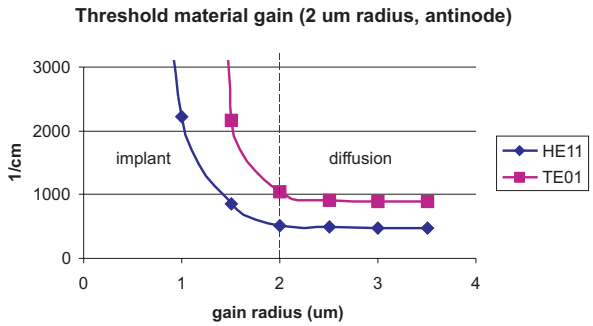

Fig. 14. Threshold material gain for the HE_{11} and the TE_{01} mode as a function of gain diameter.

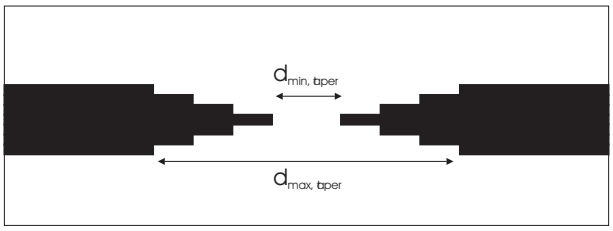

Fig. 15. Tapered oxide aperture.

which lase only in the fundamental mode, a desirable property for imaging or high-speed modulation.

Fig. 14 shows the simulated behavior of such a device, starting from the USC VCSEL structure with a 2 μm radius antinode oxide. The dashed line corresponds to a gain diameter equal to the oxide diameter, so to the right of this line we have situations where carrier diffusion increases the effective gain diameter. To the left of the line, the gain diameter is smaller than the oxide aperture, e.g. due to the presence of a proton-implantation with a smaller diameter. Obviously, decreasing the gain area leads to higher thresholds, both for the fundamental and the higher order mode. However, the relative threshold difference between these modes also becomes higher, leading to increased modal stability. Clearly, for practical applications there is a trade-off to be made between this increased modal stability and the higher threshold for the fundamental mode.

F. Tapered-oxide VCSELs

By incorporating several layers with different Al contents and by exploiting the strong dependence of oxidation rate on Al content, one can fabricate oxide apertures which are tapered rather than abrupt [17] (fig. 15). Compared to an abrupt oxide with equal thickness, a tapered oxide will provide lower confinement, but because the index change is much more gradual, scattering losses will be lower.

We illustrate this by replacing the abrupt thin oxides in the USC VCSEL with linearly tapered oxides. The inner taper radius is kept fixed at 2 μm, the outer radius is increased from 2 μm (no taper - abrupt oxide) to 3 μm. The linear profile is approximated by a staircase profile consisting of 7 steps (fig. 15). For the gain radius 3 μm is assumed. The simulation results are shown in fig. 16. For the node oxide, which already had a low confinement to start with,

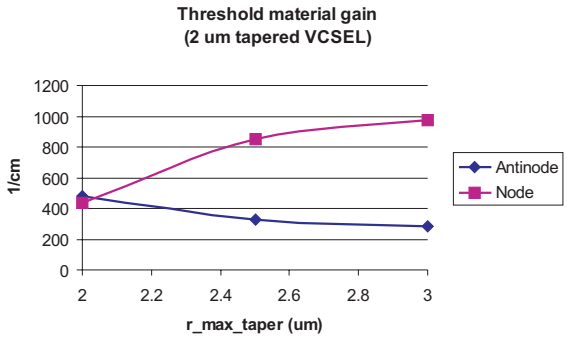

Fig. 16. Threshold material gain for a tapered VCSEL.

the even lower confinement caused by the tapering is so detrimental that the threshold goes up. Things are different for the antinode oxide, where the lower scattering outweighs the increased diffraction losses. Thresholds for the tapered antinode oxide are even lower than those of the abrupt oxide.

Clearly, this is only the tip of the iceberg, because careful control of the growth techniques and the oxidation process can provide much more sophisticated taper profiles than linear ones, like parabolic or asymmetric profiles. It is even hoped that the 'perfect' taper structure can be designed, which will act as a perfect lens that will focus the beam on a narrow spot inside the active region, without any scattering or diffraction losses [18]. Such devices could potentially have extremely low threshold currents. This is a promising area for further research. However, engineering the perfect VCSEL cavity will not be trivial because at this level of sophistication, the precise carrier diffusion profiles will have to be taken into account, in addition to other effects like thermally induced refractive index changes.

IV. Conclusion

We presented a novel optical VCSEL model based on vectorial eigenmode expansion and perfectly matched layers. Diffraction and scattering losses of VCSELs can be modeled accurately because of the presence of absorbing boundary conditions. Despite being fully rigorous and vectorial, the computational requirements of the model are still relatively modest, with run times expressed in the order of a few minutes.

This model can be used to study the threshold material gain, field profiles and modal stability of a large variety of different VCSEL designs. We illustrated that designing a confinement structure in VCSELs involves a delicate balance between diffraction and scattering losses, between the conflicting demands of high confinement inside the confining structure and small refractive index steps to reduce scattering for light entering the confining structure. Moreover, these issues cannot be considered in isolation from the rest of the VCSEL design: other aspects like cavity length or carrier diffusion have to be taken into account.

Acknowledgments

Peter Bienstman acknowledges support from the Flemish National Fund for Scientific Research (FWO - Vlaanderen) through a doctoral fellowship. Parts of this work were also carried out in the context of the Belgian DWTC project IUAP-IV-13.

References

[1] D. Huffaker and D. Deppe, "Intracavity contacts for low-threshold oxide-confined vertical-cavity surface-emitting lasers," *IEEE Photon. Technol. Lett.*, vol. 11, no. 8, pp. 934–936, 1999.

[2] M. Grabherr, M. Miller, R. Jager, R. Michalzik, U. Martin, H.J. Unold, and K.J. Ebeling, "High-power VCSEL's: Single devices and densely packed 2-D-arrays," *IEEE J. Sel. Top. Quantum Electron.*, vol. 5, no. 3, pp. 495–502, 1999.

[3] P. Bienstman, R. Baets, J. Vukusic, A. Larsson, M. Noble, M. Brunner, K Gulden, P. Debernardi, L. Fratta, G.P. Bava, H. Wenzel, B. Klein, O. Conradi, R. Pregla, S. Riyopoulos, J.-F. P. Seurin, and S.L. Chuang, "Comparison of optical VCSEL models on the simulation of oxide-confined devices," *IEEE J. Quantum Electron.*, 2001, submitted.

[4] M.J. Noble, J.P. Loehr, and J.A. Lott, "Quasi-exact optical analysis of oxide apertured microcavity VCSEL's using vector finite elements," *IEEE J. Quantum Electron.*, vol. 34, no. 12, pp. 2327–2339, 1998.

[5] B. Klein, L.F. Register, K. Hess, D.G. Deppe, and Q. Deng, "Self-consistent Green's function approach to the analysis of dielectrically apertured vertical-cavity surface-emitting lasers," *Appl. Phys. Lett.*, vol. 73, no. 23, pp. 3324–3326, 1998.

[6] B. Demeulenaere, P. Bienstman, B. Dhoedt, and R. Baets, "Detailed study of AlAs-oxidized apertures in VCSEL cavities for optimized modal performance," *IEEE J. Quantum Electron.*, vol. 35, no. 3, pp. 358–367, 1999.

[7] P. Bienstman and R. Baets, "Optical modelling of photonic crystals and VCSELs using eigenmode expansion and perfectly matched layers," *Opt. Quantum Electron.*, 2001, accepted.

[8] P. Bienstman, H. Derudder, R. Baets, F. Olyslager, and D. De Zutter, "Analysis of cylindrical waveguide discontinuities using vectorial eigenmodes and perfectly matched layers," *IEEE Trans. Microwave Theor. Tech.*, vol. 49, no. 2, pp. 349–354, Feb. 2001.

[9] J.-P. Bérenger, "A perfectly matched layer for the absorption of electromagnetic waves," *Journ. Comput. Phys.*, vol. 114, no. 1, pp. 185–200, 1994.

[10] W.C. Chew, J.M. Jin, and E. Michielssen, "Complex coordinate stretching as a generalized absorbing boundary condition," *Microwave Opt. Technol. Lett.*, vol. 15, no. 6, pp. 363–369, 1997.

[11] F.L. Teixeira and W.C. Chew, "Systematic derivation of anisotropic PML absorbing media in cylindrical and spherical coordinates," *Microwave Guided Wave Lett.*, vol. 7, no. 11, pp. 371–373, 1997.

[12] K.L. Lear, R.P. Sneider, K.D. Choquette, S.P. Kilcoyne, J.J. Figiel, and J.C. Zolper, "Vertical cavity surface emitting lasers with 21% efficiency by metalorganic vapor phase epitaxy," *IEEE Photon. Technol. Lett.*, vol. 6, no. 9, pp. 1053–1055, 1994.

[13] R.S. Geels, S.W. Corzine, and L.A. Coldren, "InGaAs vertical-cavity surface-emitting lasers," *IEEE J. Quantum Electron.*, vol. 27, no. 6, pp. 1359–1367, 1991.

[14] J.M. Dallesasse, N. Holonyak, A.R. Sugg, T.A. Richard, and L. El-Zein, "Hydrolyzation oxidation of $Al_xGa_{1-x}As$/AlGaAs quantum well heterostructures and superlattices," *Appl. Phys. Lett.*, vol. 57, no. 26, pp. 2844–2846, 1990.

[15] A.E. Bond, P.D. Dapkus, and J.D. O'Brien, "Design of low-loss single-mode vertical-cavity surface-emitting lasers," *IEEE J. Sel. Top. Quantum Electron.*, vol. 5, no. 3, pp. 574–581, May 1999.

[16] J.-F. P. Seurin, G. Liu, S.L. Chuang, L.M.F. Chirovsky, W.S. Hobson, and J. Lopata, "Modal competition in implant-apertured index-guided vertical-cavity surface-emitting lasers," *Appl. Phys. Lett.*, vol. 77, no. 23, pp. 3686–3688, Dec. 2000.

[17] E.R. Hegblom, N.M. Margalit, A. Fiore, and L.A. Coldren, "High-performance small vertical-cavity lasers: A comparison of measured improvements in optical and current confinement in devices using tapered apertures," *IEEE J. Sel. Top. Quantum Electron.*, vol. 5, no. 3, pp. 553–560, May 1999.

[18] M.J. Noble, P. Sotirelis, J.A. Lott, and J.P. Loehr, "Optical physics of VCSEL tapered oxide apertures," in *Proc. SPIE vol. 3944*, R.H. Binder, P. Blood, and M. Osinski, Eds., 2000, pp. 252–263.

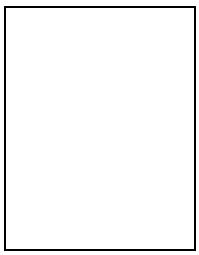

Peter Bienstman was born in Ghent, Belgium, in 1974. He received a degree in electrical engineering from Ghent University, Belgium, in 1997 and a PhD from the same university in 2001, at the Department of Information Technology (INTEC). His research interests include the modeling of optical structures, notably resonant-cavity light-emitting diodes, vertical-cavity surface-emitting lasers and photonic crystal structures. He has published several papers and has one patent application pending. He is a student member of IEEE-LEOS.

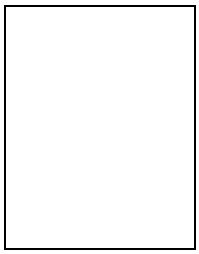

Roel Baets received the degree in electrical engineering from Ghent University, Belgium, in 1980. He received the M.Sc. degree in electrical engineering from Stanford University in 1981 and the Ph.D. degree from Ghent University in 1984. Since 1981 he has been with the Department of Information Technology (INTEC) of Ghent University. Since 1989 he is a professor in the engineering faculty of Ghent University. From 1990 till 1994 he has also been a part-time professor at the Technical University of Delft, The Netherlands. Roel Baets has worked in the field of III-V devices for optoelectronic systems. With about 200 publications and conference papers he has made contributions to the design and fabrication of semiconductor laser diodes, passive guided wave devices, PICs and microoptic components. He leads the Optoelectronic components and systems group at Ghent University-IMEC, working on photonic devices for optical communication and optical interconnect. Roel Baets is a member of the Optical Society of America, IEEE-LEOS, SPIE and the Flemish Engineers Association. Currently he is chairman of the IEEE-LEOS-Benelux chapter.